Image System Solution for Store Aerodynamics with Interference—Part II

Fred W. Martin*
Auburn University, Auburn, Ala.

and

Kenneth B. Walkley†
LTV Aerospace Corporation, Hampton Technical Center, Hampton, Va.

The mutual aerodynamic interference problem for external aircraft-stores has been analyzed using the image system technique. To facilitate this analysis it has been assumed that small perturbation solutions are valid. It is further assumed that the external stores are slender, axisymmetric bodies and that the mutual interference can be analyzed by first assuming a cross-flow solution. Both body-body and wing-body interference solutions have been obtained. The first were considered in Part I of this paper. For the wing-body solution, the image systems in the cross-flow plane consist of vortex pairs appropriately located by using the Milne-Thomson circle theorem. The strengths of the image vortex system are then determined by satisfying the body boundary conditions at designated control points on the external stores. Good agreement has been found between the theoretical and experimental results.

Nomenclature

C_p = pressure coefficient
c = wing chord
F_u, F_v, F_w = influence coefficients
K_i' = nondimensional image strength
K_i = strength of image horseshoe vortex
M_∞ = Mach number of freestream flow
N = number of points on body
P_b, Q_b, R_b = body reference coordinates (origin at body nose)
P_n, Q_n, R_n = coordinates which locate a particular horseshoe vortex
Q_o, R_o = lateral and vertical vortex-body separation distance (Fig. 2)
P, Q, R = wing Cartesian coordinate system
r = radius of body (Fig. 1)
r_1, r_2 = radii which locate vortices (Fig. 1)
r_j = radius to j^{th} point in flowfield at x_j location
s = local image vortex semispan (Fig. 4)
s_w = semiwidth of wing vortices (Fig. 4)
s_j = local image vortex semispan at the x_j location
u, v, w = nondimensional velocity perturbations in the ξ, η, ζ directions
u', v', w' = perturbation velocities due to wing vortices
u_∞ = freestream velocity
x = axial coordinate along body
x_j = axial distance to j^{th} point
u'', φ'' = perturbation velocities due to source distribution
α_w, α = wing angle of attack
δ_1, δ_2 = radii to vortices in image system (Fig. 2)
Δx = length increment between point sources (Fig. 2)
Γ = strength of planar vortices
Γ'_n = nondimensional vortex strength
ξ, η, ζ = Cartesian coordinate system fixed in body
ξ_i, η_i, ζ_i = coordinates to i^{th} point
ϕ = dihedral angle for a given image vortex element (Fig. 4)
ϕ_j = dihedral angle for a given image vortex element at the j^{th} point
$\phi_1 \phi_2$ = dihedral angle for location δ_1 and δ_2, respectively (Fig. 4)
ϕ_j = meridional angles for which boundary conditions are exactly satisfied
ψ = arbitrary meridional angle
$\bar{(\ )}$ = property associated with leading edge vortices
$(=)$ = property associated with trailing edge vortices

Received January 15, 1974; revision received October 18, 1974. Presented as Paper 35 at the Aircraft/Stores Compatibility Symposium, Sacremento, Calif., September 18-20, 1973. This paper is related to work supported by USAF, Eglin Air Force Base, under Contract F08635-71-C-0090.

Index categories: Aircraft Aerodynamics (Including Component Aerodynamics); Subsonic and Transonic Flow.

*Professor, Aerospace Engineering Department. Member AIAA.

†Aerodynamics Engineer; formerly graduate student, Aerospace Engineering Department, Auburn Univeristy, Auburn, Ala.

Introduction

THE subject solution which was discussed for 2, 3, and 4 bodies in Ref. 1 is extended in this paper to the wing-pylon-body case. Current work involves extension to the wing-pylon-4 body case. Essentially, the solution involves the generation of the mutual interference using small perturbation solutions for the isolated bodies and superposition of an appropriate image system of source and/or vortex singularities. The primary goal of this work is to be able to accurately predict the trajectory of a store from an aircraft in an interference flowfield.

In a manner similar to the technique used for the body-solution,[1] the wing is modeled as a system of rectangular horseshoe vortices[2] while the body is generated by a three-dimensional source distribution.[1] The resulting nonuniform flowfield of the wing is then used to determine a vortex image system in the body which preserves the body boundary condition. The necessary image system is found by applying the Milne-Thomson circle theorem to a pair of counter-rotating planar vortices in the vicinity of a circle.[3] The store induced loads on the wing and pylon are not accounted for in this paper as a preliminary study showed this effect to be small.[3]

Vortex Image System

A vortex image system must be constructed in the axisymmetric body so that the nonuniform flow boundary conditions resulting when the body is in the interference flowfield of the wing will be satisfied. Such an image system may be found by applying the method of images commonly employed in two-dimensional flow theory to a series of cross-flow planes in the body as follows.

Consider first two equal strength counter-rotating planar vortices in the vicinity of a circle as shown in Fig. 1. Application of the Milne-Thomson circle theorem [3] shows that to preserve the boundary of the circle as a streamline in this nonuniform flowfield, two image vortices must be placed in the circle for each vortex outside the circle; one vortex of equal strength at the center of the circle and another of equal and opposite strength at the inverse point. Because the vortices exterior to the circle are of equal but opposite strength, the image vortices at the center of the circle exactly cancel so that the two-dimensional image system consists only of the vortices at the inverse points δ_1 and δ_2 (Fig. 2).

This two-dimensional result may now be adapted to the full three-dimensional problem by considering a single rectangular horseshoe vortex on a lifting-surface at angle-of-attack α near the body (Fig. 2). The circle theorem may be applied locally in successive cross-flow planes to obtain continuous distributions of the two-dimensional displacement distances $\delta_1(x)$ and $\delta_2(x)$ based on the local vertical separation distances R_o between the body center line and the horseshoe vortex filaments. At each axial station coinciding with the point sources along the body center line, two semi-infinite linear vortex filaments of strength K_i are located at the local two-dimensional displacement distances. These filaments are parallel to the body axis and extend downstream to infinity, and half of one axial increment ($\Delta x/2$) in the upstream direction. Here they are joined by a linear filament of like strength to form a rectangular horseshoe vortex. A second horseshoe vortex of strength $-K_i$ is added at a distance (Δx) downstream from the leading vortex crosspiece as shown in Fig. 2. The addition of this opposite strength trailing vortex effectively cancels the trailing legs of the leading vortex except for the length Δx between the crosspieces of the vortices. Successive application of this scheme to the N circular cross-flow planes coinciding axially with the N point sources results in N rectangular vortex elements centered about the point sources.

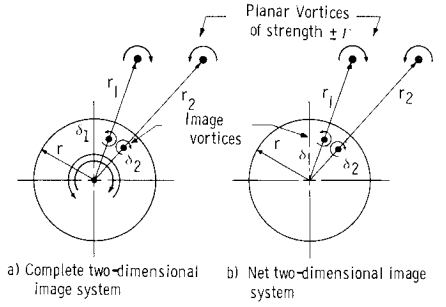

Fig. 1 Two-dimensional image system for a pair of counter-rotating vortices.

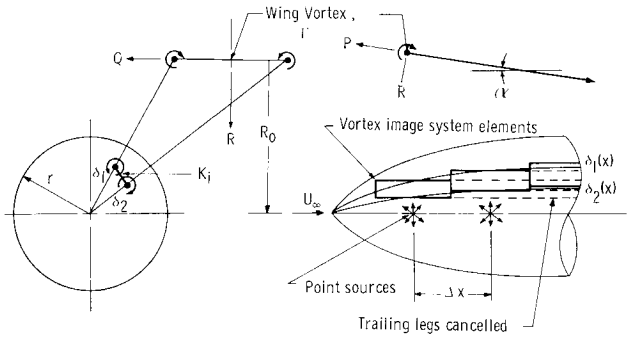

Fig. 2 Three-dimensional image system for a pair of counter-rotating vortices.

Image System Geometry

The local geometry in a given cross-section of the body may be used to determine the coordinates, semispans, and dihedral angles of the image system vortices. Consider a single horseshoe vortex of dihedral angle ϕ_w and semispan s_w in the near vicinity of an axisymmetric body as shown in Figs. 3 and 4. If a PQR coordinate system is fixed in the wing which is at angle-of-attack α, then a particular horseshoe vortex may be located by coordinates (P_n, Q_n, R_n) while the tip of the body nose has reference coordinates (P_b, Q_b, R_b) as shown. The image vortices are located within the circular cross section, of radius r, at the inverse points, δ_1 and δ_2 along the lines r_1 and r_2 drawn from the center of the body to the tips of the wing vortex. Using the notation of Refs. 2 and 3, and the geometry from Figs. 4 and 5, the appropriate expressions are as follows:

$$\delta_1 = \frac{r^2}{r_1} = \frac{r^2}{[(R_o - s_w \sin\phi_w)^2 + (Q_o - s_w \cos\phi_w)^2]^{1/2}} \quad (1)$$

$$\delta_2 = \frac{r^2}{r_2} = \frac{r^2}{[(R_o + s_w \sin\phi_w)^2 + (Q_o + s_w \cos\phi_w)^2]^{1/2}} \quad (2)$$

where the local vertical and lateral separation distance between the body and the center line of the horseshoe vortex are

$$R_o = R_b - R_n \cos\alpha + (P_b - x)\cos\alpha \sin\alpha + [(P_b - x)\sin^3\alpha/\cos\alpha] \quad (3)$$

$$Q_o = Q_b - Q_n \quad (4)$$

The local image vortex semispan is

$$s = 0.5[\delta_1^2 + \delta_2^2 - 2\delta_1\delta_2\cos(\theta_1 - \theta_2)]^{1/2} \quad (5)$$

where

$$\theta_1 = \tan^{-1}\left[\frac{R_o - s_w \sin\phi_w}{Q_o - s_w \cos\phi_w}\right] \quad (6)$$

$$\theta_2 = \tan^{-1}\left[\frac{R_o + s_w \sin\phi_w}{Q_o + s_w \cos\phi_w}\right] \quad (7)$$

The dihedral angle for a given image vortex element is then

$$\phi = \tan^{-1}\left[\frac{\delta_2 \sin\theta_2 - \delta_1 \sin\theta_1}{\delta_2 \cos\theta_2 - \delta_1 \cos\theta_1}\right] \quad (8)$$

where ϕ is considered positive if the plane of the image element has been rotated from the Q axis toward the R axis.

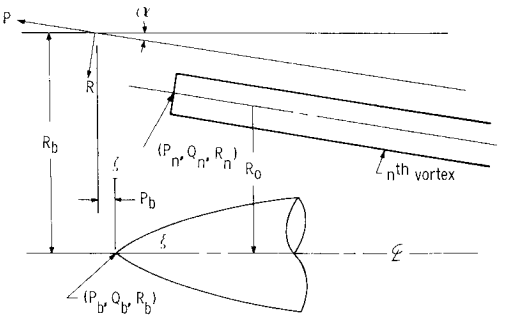

Fig. 3 Geometry for a single horseshoe vortex.

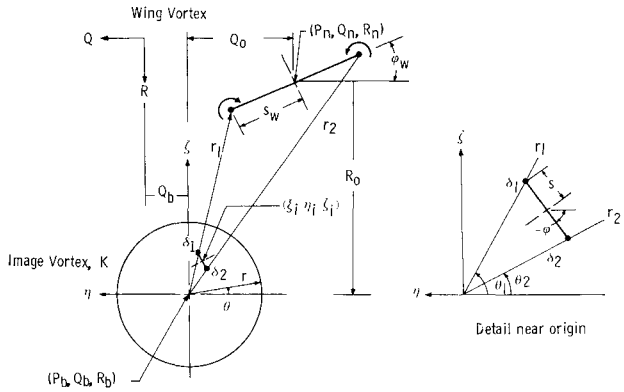

Fig. 4 Vortex-body image system.

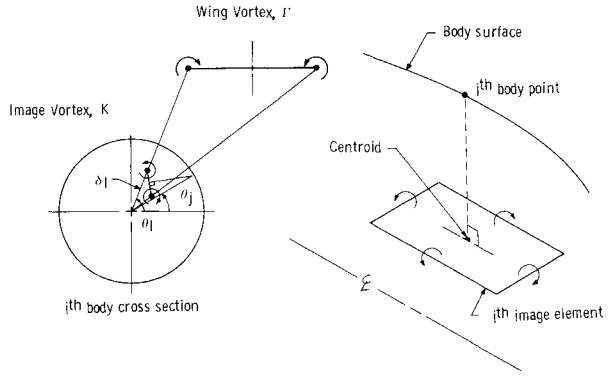

Fig. 5 Geometric relations for the boundary condition angles θ_j.

The image dihedral angle shown in Fig. 2 is thus negative. The coordinates of the mid-point of the crosspiece of a given image element in the body axis system are

$$\xi_i = x \mp \Delta x/2 \tag{9}$$

$$\eta_i = -\delta_1 \cos\theta_1 - s\cos\phi \tag{10}$$

$$\zeta_i = \delta_1 \sin\theta_1 + s\sin\phi \tag{11}$$

where $(\mp)$ refers to the leading and trailing vortices, respectively, of the image element.

Body Boundary Condition

The unknown image system vortex strengths may be found by considering the boundary condition at the body surface which again requires that the flow be tangential. Equation (2) from Ref. 1 is

$$dr/dx = v_r/1 + u \tag{12}$$

Note that in this case v_r and u represent the total radial and axial velocity perturbations due to the single wing vortex under consideration, the point source distribution, and the vortex image system. Each of these velocities must be measured relative to the (ξ,η,ζ) coordinate system fixed in the body. If θ is a meridional angle measured in the same sense as θ_1 and θ_2, the total perturbations at the j^{th} point on the surface may be expressed as

$$v_{r_j} = v''_{r_j} + u'\sin\alpha\sin\theta - (w'\cos\alpha + w)\sin\phi - (v' + v)\cos\phi \tag{13}$$

$$u_j = u'' - u'\cos\alpha - u - w'\sin\alpha \tag{14}$$

The coordinates of the body points relative to a given wing vortex are known from the wing/body geometry so that the velocities induced at the j^{th} body point by a wing vortex of known strength may be determined directly using the influence coefficients as given in Refs. 2-4. Likewise, the radial and axial perturbations at the body points due to the point sources are known. The only remaining unknowns, then, are the velocities induced by the vortex image system. These velocities may be conveniently separated into the components induced by the leading and trailing horseshoe vortices:

$$u_j = \bar{u}_j + \bar{\bar{u}}_j \tag{15}$$

$$v_j = \bar{v}_j + \bar{\bar{v}}_j \tag{16}$$

$$w_j = \bar{w}_j + \bar{\bar{w}}_j \tag{17}$$

By definition, the sense of the trailing vortices, K_i, is opposite to that of the corresponding leading vortices, $\bar{K}_i$, thus

$$\bar{\bar{K}}_i \equiv -\bar{K}_i \tag{18}$$

so that the trailing legs are cancelled. Then for n image system vortex elements the velocities induced at the j^{th} body point are

$$u_j = \sum_{i=1}^{N} (\bar{F}_{u_{j,i}} - \bar{\bar{F}}_{u_{j,i}})\bar{K}'_i \tag{19}$$

$$v_j = \sum_{i=1}^{N} (\bar{F}_{v_{j,i}} - \bar{\bar{F}}_{v_{j,k}})\bar{K}'_i \tag{20}$$

$$w_j = \sum_{i=1}^{N} (\bar{F}_{w_{j,i}} - \bar{\bar{F}}_{w_{j,i}})\bar{K}'_i \tag{21}$$

where the influence coefficients F_u, F_v, are of the same form as for the wing vortex system. Substituting Eqs. (19 - 21) into (12) and (13) and simplifying gives:

$$\frac{dr_j}{dx_j}(1 + u''_j - u'_j\cos\alpha - w'_j\sin\alpha) - v''_{r_j} - u'_j\sin\alpha\sin\theta_j + w'_j\cos\alpha\sin\theta_j + v'_j\cos\theta_j = \sum_{i=1}^{N}\left[\frac{dr_j}{dx_j}(\bar{F}_{u_{j,i}} - \bar{\bar{F}}_{u_{j,i}}) - (\bar{F}_{v_{j,i}} - \bar{\bar{F}}_{v_{j,i}})\cos\theta_j - (\bar{F}_{w_{j,i}} - \bar{\bar{F}}_{w_{j,i}})\sin\theta_j\right]\bar{K}'_i \tag{22}$$

where $j = 1,2,3 \ldots N$ specifies a given body point. Note that only one angle θ_j may be specified for a given cross section so that the boundary condition is satisfied exactly only at that particular point. Application of Eq. (22) to the N body points results in a system of N linear algebraic equations which may be solved for the N unknown image system vortex strengths. These strengths may then be used to calculate the induced velocities at any point on the body surface or in the surrounding flowfield.

Determination of the Boundary Condition Angles

The strength distribution of the vortex image system is found by employing Eq. (22) at thirty points on the body surface coinciding axially with the thirty point sources. The angles θ_j $(j = 1,2, \ldots 30)$ must first be specified, however. The choice of these angles would appear to be quite arbitrary in that the purpose of the image system is to maintain the tangent-flow boundary condition at all meridional angles once the solution has been obtained for a given angle. It has been found, however, that the choice of the angles θ_j does influence the numerical solution and, in some cases, determines whether or not a valid solution may be obtained. The θ_j angles may not be arbitrarily specified because the rectangular image elements are strictly three-dimensional. Hence the induced velocities are directly dependent on the location of a

particular point under consideration. It is possible, then, to choose the boundary points (i.e., the angles θ_j) such that the induced velocity does not properly represent the contributions from each of the four vortex filaments comprising the rectangular image elements. Such a situation occurs for a pylon vortex ($\phi_w = \pm 90°$) whose image elements have a dihedral angle of $\phi = \pm 90°$. If the boundary condition is satisfied along the line $\phi_j = +90°$, an invalid solution occurs because only tangential velocities are induced at the specified control points. The resulting image system strengths do not properly reflect the need to cancel nontangential components at other points around the body. The tangent-flow boundary condition then is not preserved for other meridional angles.

To avoid the difficulties presented above and to obtain a systematic method for locating the body points, the following scheme has been devised: The influence of each vortex filament in a given image element may be appropriately considered if the angles θ_j are chosen as shown in Fig. 5. A line is drawn perpendicular to the image element at its centroid and projected to the body surface on the downflow side of the element. The exact θ_j values in the j^{th} cross-flow plane may then be determined by solving the equation of this perpendicular line at the point where it intersects the circle. The result is

$$\theta_j = \phi_j + \cos^{-1}\left(\frac{\delta_{I_j}\cos(\theta_{I_j} - \phi_j) + s_j}{r_j}\right] \qquad (23)$$

Application of Eq. (23) does, in general, give a different value for θ_j at each body station. Equation (21) may now be solved for the vortex image strengths.

Numerical Solution for the Vortex Image System

To evaluate a vortex image system numerically, several cases representative of the actual conditions arising in the application of the theory to the finite wing discussed in the next Section have been studied. In each case, the axisymmetric body is aligned parallel to the freestream direction while the single horseshoe vortex under consideration is at an angle of attack of either 2° or 4°. The body reference coordinates (P_b, Q_b, R_b) are measured as indicated in Figs. 3 and 4 where the (P,Q,R) coordinate system is now fixed in the horseshoe vortex as shown in Fig. 2.

The calculated image system vortex strengths for a wing vortex at 2° angle of attack are shown in Fig. 6. The θ_j angles for this case decrease from 142° at the nose to 138° along the constant radius midsection and then increase along the tail to 149.° The results of the two-dimensional theory have, to a certain extent, been carried over to the three-dimensional case in that the magnitudes of the image strengths tend approximately to that of the wing vortex over that portion of the body downstream of the crosspiece of the wing vortex. Figures 7 and 8 compare the actual body slope to the slope of the streamline at the body surface. Typical results for meridional angles of $\psi = 110°$ are presented. (To avoid confusion, ψ is taken to represent a given meridional angle while θ_j designates the angles at which the boundary condition is exactly satisfied. Note that ψ is measured from the same reference as θ_j). The agreement of the actual and calculated slopes is excellent and is typical of the correlation which is obtained for any meridional angle. In no case does the error in

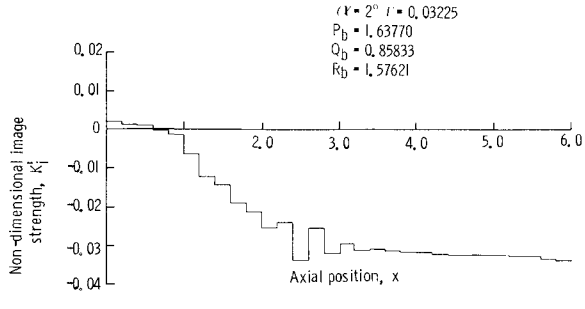

Fig. 6 Typical vortex strength distribution for the body image system for a wing vortex.

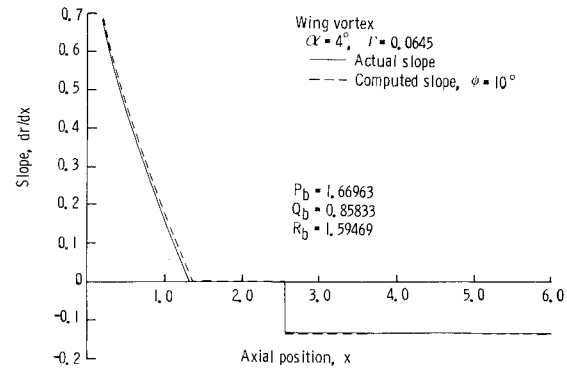

Fig. 7 Comparison of actual and computed body slope, $\psi = 10.°$

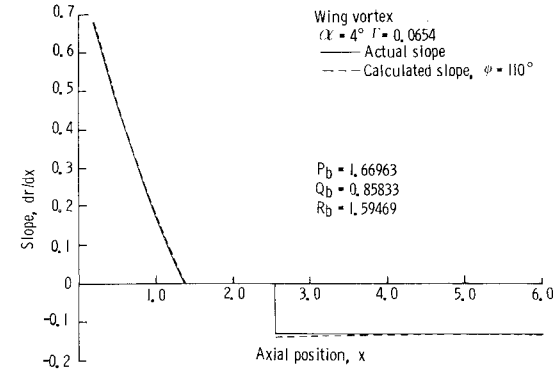

Fig. 8 Comparison of actual and computed body slope, $\psi = 110.°$

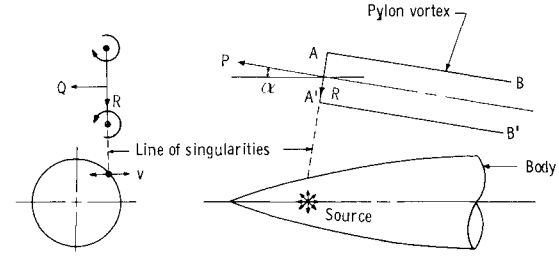

Fig. 9 Line of singularities from a pylon vortex intersecting the body.

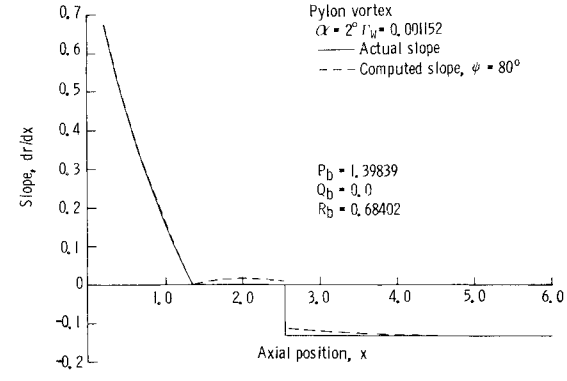

Fig. 10 Comparison of actual and computed body slopes, $\psi = 80.°$

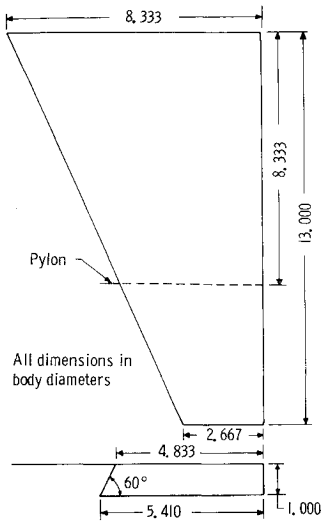

Fig. 11 Flat-plate wing-pylon model.

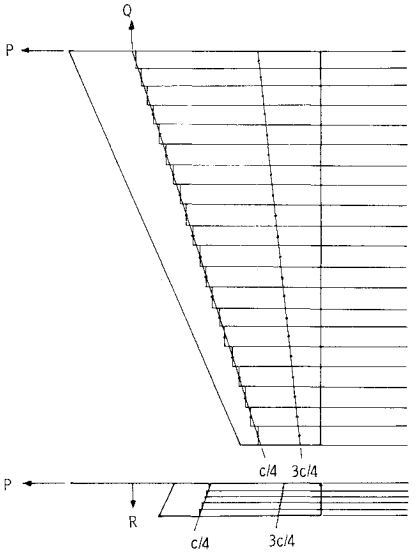

Fig. 12 Horseshoe vortex system for wing and pylon.

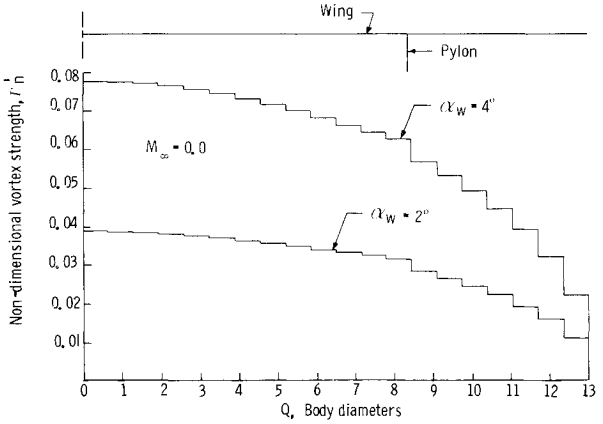

Fig. 13 Vortex strength distribution for the wing.

the calculated body slope exceed $\pm 1°$. Errors of this magnitude are well within the small disturbance theory assumptions made in order to express the pressure coefficient in terms of the perturbation velocities.

Similar results are obtained for a horseshoe vortex oriented to represent a portion of a pylon surface with dihedral angle $\phi = \pm 90°$. In this case, however, special consideration must

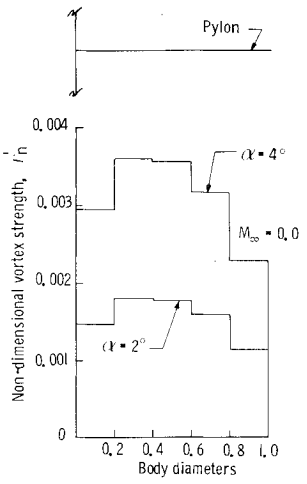

Fig. 14 Vortex strength distribution along the pylon.

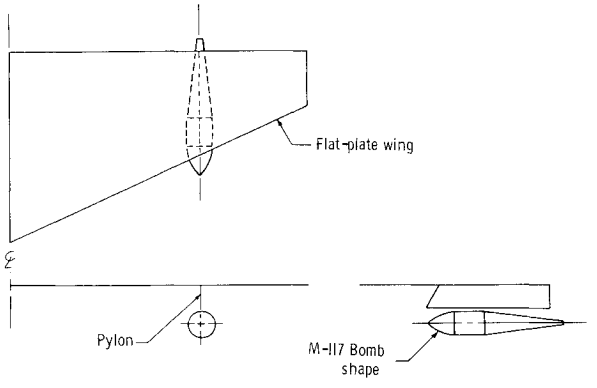

Fig. 15 Schematic of flat-plate wing with M-117 bomb shape.

be given to the line of singularities extending from the crosspiece of the pylon vortex (Fig. 9). Along this line the velocities induced by vortex filament AA' are indeterminate, but the contributions from filaments AB and $A'B'$ are finite. The influence coefficients for a horseshoe vortex must be modified so that only the influence of filaments AB and $A'B'$ is considered.

A typical result for a pylon vortex very near the body is given in Fig. 10. In this case, the θ_j values range from 167° at the nose to 128° at the midsection, and then increase along the tail to 175.° As for the wing vortex, the image system strengths tend to the value of the pylon vortex, and the calculated body slope agrees very well with the actual values except along the body midsection. The error in slope is still less than +1,° however. Results for other pylon vortices show essentially no error in slope so that the body boundary condition is preserved by the image system.

Analysis of a Wing-Pylon-Body Combination

To evaluate the aerodynamic interference effects of a wing with pylons, an arbitrary swept wing has been studied. The geometry of this wing is shown in Fig. 11 where all dimensions are in nondimensional body diameters. In all cases, the body is oriented directly beneath the pylon such that the lower tip of the pylon and the body nose coincide axially. Such a position represents the store location immediately after release from the pylon.

Solution for the Isolated Wing

The wing is approximated as a system of horseshoe vortices as shown in Fig. 12. As pointed out in Ref. 2, the use of equal span vortices of semiwidth $s_w = 0.0250$ $(b/2)$ generally provides satisfactory results. Applying this guide to the wing

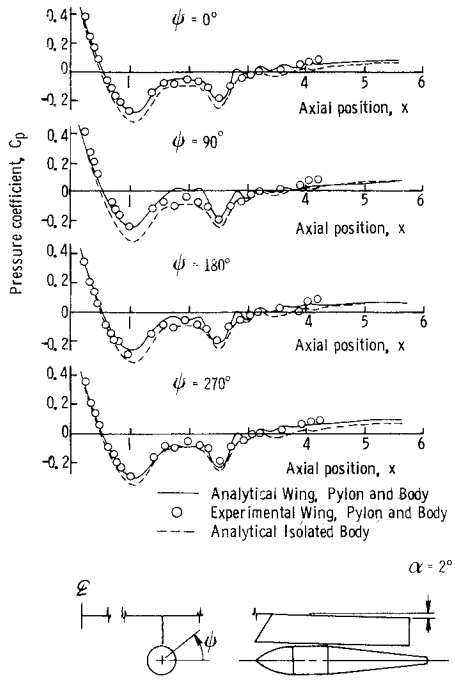

Fig. 16 Comparison of theory with experiment for wing-pylon-body interference.

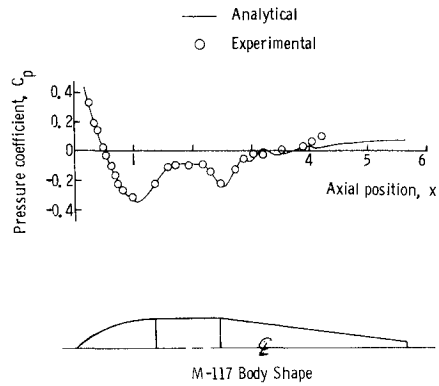

Fig. 17 Pressure distribution for axisymmetric body.

and pylon under consideration results in 50 horseshoe vortices being used; 40 on the wing and 5 on each pylon. The vortex strength distribution on the wing and pylons uses the method in Ref. 2. The results for wing angles of attack of 2° and 4° are presented in Figs. 13 and 14 for the wing and pylon surfaces, respectively. A discontinuity in the wing strength distribution occurs as expected at the pylon location. The pylon suppresses the spanwise component of the induced flow causing a finite jump in the vortex strength distribution. A similar trend is seen for the pylon vortex strength distribution in Fig. 14. The wing likewise suppresses the normal component of the flow so that a discontinuity in the pylon vortex strength distribution occurs near the wing. Finally, the interference flowfield may be generated by constructing the appropriate image system for each horseshoe vortex on the wing and pylon surfaces.

Results and Conclusions

The theoretical pressure distribution obtained using this analytical technique for a wing-pylon-body solution has been compared with experiment. The experiment utilized a flat-plate wing with a straight taper planform with an M-117 bomb shape under a flat-plate pylon. The theoretical pressure distribution was calculated from the velocity ratios where the velocity terms represent the total induced flow due to all of the vortex image systems, the system of wing and pylon vortices, and the point source distributions. Because the influence at a given point diminishes rapidly with increasing distance to that point, it is unnecessary to consider those wing vortices which are located three or more reference diameters from the body. The velocities induced by such vortices are negligible compared to those induced by vortices in the near vicinity of the body. The effect of a similar body carried on the opposite pylon is likewise negligible as the two bodies are, in this case, separated by more than 16 reference diameters. This simplification greatly reduces the time required for the numerical solution.

The experimental data were obtained from wind tunnel tests using a half-span flat plate wing (Fig. 15) and an axisymmetric body at low subsonic speeds. The body could be rotated a full 360° so that pressure distributions for any meridional angle could be measured. The body was aligned parallel to the freestream direction while pressure data for wing angles of attack of 2° and 4° were obtained.

The predicted and measured body pressure distributions for a wing at an angle of attack of 2° are compared in Fig. 16. These results are for meridional angles of $\psi = 0°$, 90,° 180,° and 270.° Some deviations occur along the constant radius midsection of the body, but in general the analytical pressure coefficients are in good agreement with experimental values for all meridional angles. To show the relative dependence of the pressure distribution on ψ, the theoretical pressure distribution for the isolated body has been included in Fig. 16. The validity of the solution for the isolated body is shown in Fig. 17.

References

[1] Martin, F. W., et al., "Image System Solution for Store Aerodynamics with Interference—Part I," this issue, page 151. (An additional 6 references are listed there).

[2] Blackwell, J. A., "A Finite-Step Method for Calculation of Theoretical Load Distribution for Arbitrary Lifting-Surface Arrangements at Subsonic Speeds," TN D-5335, July 1969, NASA.

[3] Walkley, K.B., "Aerodynamic Interference of Wing-Pylon-Body Combinations at Low Subsonic Speeds," MS thesis, June 1973, Aerospace Engineering Department, Auburn University, Auburn, Ala.

[4] Glauert, H., *The Elements of Aerofoil and Airscrew Theory*, Cambridge University Press, Cambridge, England, 1937.